Available online at www.sciencedirect.com

ScienceDirect

Procedia Materials Science 9 (2015) 221 – 229

Procedia Materials Science

www.elsevier.com/locate/procedia

International Congress of Science and Technology of Metallurgy and Materials, SAM – CONAMET 2014

Thickness dependence of crystalline structure of Al-doped ZnO thin films deposited by spray pyrolysis

F. A. Garcés[a,*], N. Budini[a], R. D. Arce[a,b], J. A. Schmidt[a,b]

[a] *Instituto de Física del Litoral (UNL-CONICET), Güemes 3450, S3000GLN Santa Fe, Argentina*
[b] *Facultad de Ingeniería Química (UNL), Sgo. del Estero 2829, S3000AOM Santa Fe, Argentina*

Abstract

In this work, we have investigated the influence of thickness on crystalline structure of Al-doped ZnO films. Transparent conducting oxide films were grown by the spray pyrolysis technique from precursors prepared via the sol-gel method. We determined the structural properties of the films by performing X-ray diffraction and mosaicity measurements, which evidenced an increase of disorder and inhomogeneity between crystalline domains as the films thickened. This behavior was attributed to plastic deformation of the films as their thickness increased. Disorder is usually caused by internal stress in the crystalline structure of the film, which is due to diverse factors such as lattice and thermal mismatches between substrate and sample, postdeposition heat treatments, film growth parameters, film thickness, etc. Although there are several reports concerning stress-induced optical and electrical fluctuations of ZnO films, due to annealing or deposition processes, different substrates types and doping, the thickness dependence of structural characteristics is scarcely reported.

Peer-review under responsibility of the Scientific Committee of SAM–CONAMET 2014

Keywords: Mosaicity, sol-gel, thin film, zinc oxide, stress, electrical properties

1. Introduction

Intrinsic and doped ZnO thin films are currently under investigation and development for applications in opto-electronics and energy conversion. In particular, transparent and conductive Al-doped ZnO (AZO) films are being considered for manufacturing transparent electrodes in flat panel displays, solar cells and organic devices due to their high electro-optical quality, high material availability and low cost for large area applications [Hao et al. (2006); Granqvist (2007); Minami (2008)]. Many techniques have arisen to deposit ZnO films on different substrates, such as sol-gel method [Natsume and Sakata (2000)], spray pyrolysis [Lokhande and Uplane (2000)], metal-organic chemical vapor deposition [Gorla et al. (1999)], pulsed laser deposition [Choi et al. (2001)], molecular beam epitaxy [Bagnall et al. (1997)] and sputtering [Ellmer (2000)]. Among these, the spray pyrolysis method has gained increased interest during the last years due to some advantages in comparison to other methods. It is simple and easy to implement,

* Corresponding author. Tel.: +54-342-455-9174.
E-mail address: felipe.garces@santafe-conicet.gov.ar

Peer-review under responsibility of the Scientific Committee of SAM–CONAMET 2014
doi:10.1016/j.mspro.2015.04.028

produces high purity films and provides excellent control of chemical uniformity. This non-expensive method was initially developed for transparent conducting oxide deposition in solar cells applications since the process is flexible and allows simple modifications for large area depositions. Regarding the chemical spray technique, ZnO thin films are frequently deposited by pyrolytic reaction of zinc acetate dissolved in an alcoholic solution. To obtain films with low resistivity, F, In, Ga and Al are some of the most used dopants. In the case of Al, every ion of the dopant can replace a Zn atom in the structure and release a free electron, which increases the free carrier concentration [Paraguay D. et al. (2000); Rao et al. (2012)]. Up to now, Al has emerged as the most successful dopant to effectively decrease the resistivity of ZnO films, lowering it to about 2×10^{-3} Ω cm, while maintaining an average transmittance of 85% in the visible region of the spectrum [Rao et al. (2012)]. In addition, a preferential growth in either the (0 0 2) or the (1 0 1) plane is obtained, depending on the deposition conditions.

In a recent work, we have studied the effect of thickness on the structural and electrical characteristics of SnO_2:F thin films, synthesized by the sol-gel method and deposited by spray pyrolysis [Garcés et al. (2013)]. We have found a strong relation between thickness and crystalline domain misorientation or mosaicity, which also influences the electronic transport. Consequently, in the present study we have used the same methodology (i.e. sol-gel and spray pyrolysis) to deposit and study transparent conducting AZO films with different thicknesses, varying only the deposition time. The present work aims at investigating the stress arising from thickness variation and its effect on the optical properties. Also, we investigated the effect of film thickening on the evolution of morphological and electrical properties. The correlation between structural properties, mosaicity, optical and electrical properties of these films is discussed.

2. Experimental details

We synthesized the AZO ethoxylated precursors from Zn salts [Sigma-Aldrich 99.999% $Zn(O_2CCH_3)_2(H_2O)_2$, 0.2 M] and Al dopant through the sol-gel method [Znaidi (2010)]. The Al source was the $AlCl_3 \cdot 6H_2O$ compound (Sigma-Aldrich 99.0%). Subsequently, through a spray pyrolysis process we deposited AZO thin films on glass (Borofloat®) [Garcés et al. (2013)]. To fabricate samples with different thicknesses, the deposition times were varied in the range from 5 to 30 min, namely 5, 15, 20, 25 and 30 min. These times led to thicknesses of 0.43, 0.67, 0.80, 1.26 and 1.40 μm, respectively. A $(TEA)NC_6H_{15}$ (Sigma-Aldrich > 99%) solution was used as an additive for the sol-gel process. The precursors were gauged in a total volume of 100 ml by using solvents like ethanol and water. Generally, the deposition temperature used for ZnO fabrication is in the range between 380 and 500 °C [Biswal et al. (2010)]. In this work we have used a temperature of 450 °C, which was chosen after optimizing the resistivity and transparency of the deposited films. The Al concentration was fixed taking into account the fraction Al/Zn which, in this case, was 1.0%. It is worth noting that this concentration corresponds to the precursor in solution.

To have an insight on the structural characteristics of the samples we performed X-ray diffraction (XRD) measurements in the typical θ-2θ Bragg-Brentano configuration. The details concerning mosaicity measurements can be seen in Ref. [Garcés et al. (2013)]). The XRD measurements were carried out in a Shimadzu XD-D1 diffractometer, operating with the Cu Kα line (λ = 1.541 Å). Film thickness was determined by direct transmittance measurements, in a Shimadzu UV3600 spectrophotometer. Surface roughness and texture were inspected by atomic force microscopy (AFM) measurements, performed in a NANOTEC probe system.

In turn, the electrical characterization was achieved by performing Hall effect measurements, at room temperature, by the Van der Pauw method.

3. Results and discussion

AFM images are generally used to characterize the morphology of the surface, by means of root-mean-square (RMS) roughness, and to determine the grain size. Our layers presented a quite uniform surface morphology dominated by hexagonal structures, as shown in Fig. 1 for the different deposition times. The shape of the grains is shown augmented in the inset of each AFM image. At the lower right of Fig. 1 we plot the variation of RMS roughness as a function of the film thickness. Normally, RMS roughness gradually enlarges as thickness increases, which is the observed trend for our samples. As thickness reached its highest value (1.40 μm) RMS roughness grew monotonically to 65 nm. This behavior is consistent with the results obtained from XRD measurements, as will be shown

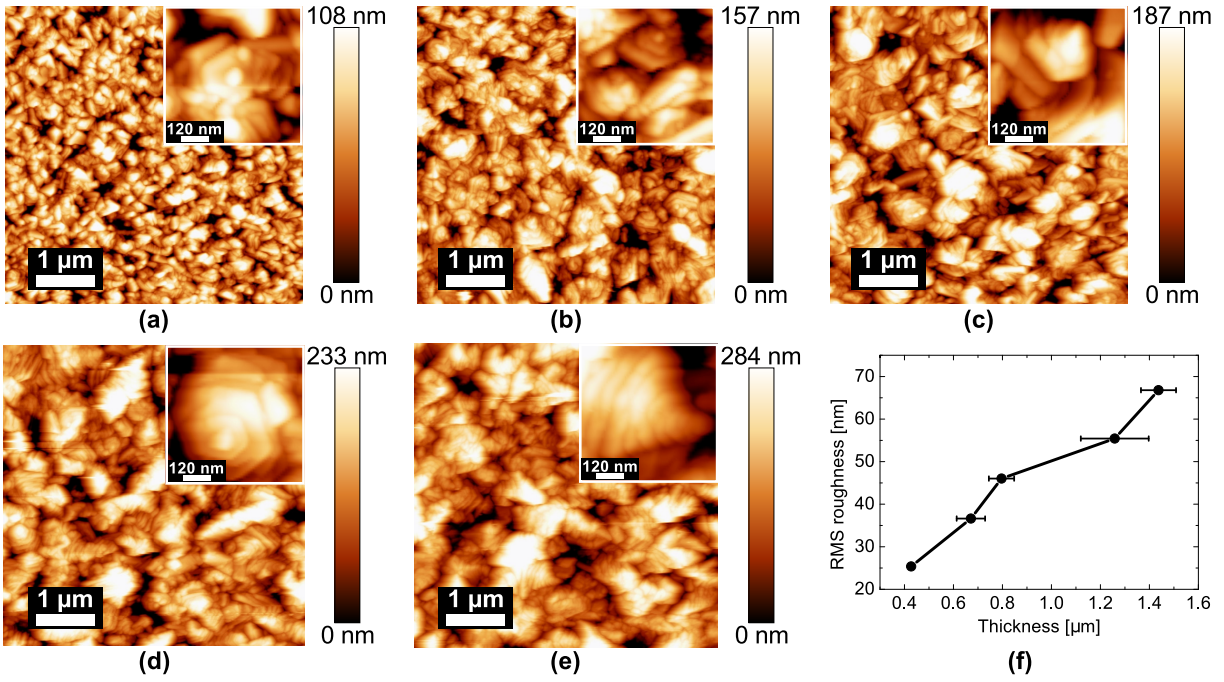

Fig. 1. Atomic force microscopy images for AZO films with different thicknesses, obtained by spray pyrolysis after a deposition time of (a) 5 min, (b) 15 min, (c) 20 min, (d) 25 min and (e) 30 min; (f) RMS roughness of the resulting films as a function of thickness.

later. The hexagonal morphology observed on the surface is attributable to oriented growth in the [0 0 2] direction of ZnO wurtzite phase [Mekhnache et al. (2011)]. RMS roughness increased for thicker samples due to the stacking of successive layers possessing these hexagonal structures oriented in different directions with respect to the substrate normal. We also observed that, besides the stacking of these hexagonal-shaped nanosheets, there was an enlargement of the hexagons that form these stacked structures. For a film thickness of around 0.6 μm (Fig. 1, 0.42 and 0.67 μm) the grains grew to about 0.2 μm. It is likely that the stacking of nanosheets, for thicknesses between 0.80 and 1.4 μm, gives place to a pyramidal structure as shown in Fig. 1 for the last three deposition times.

The changes in the shape of ZnO grains as a function of film thickness can be explained by the transformation of growth model. During the deposition of thinner films, the grains grow approximately following a 2D model [Lan et al. (2009)]. This results in the formation of hexagonal-shaped ZnO nanosheets with a high width/thickness ratio of up to 10. However, as thickness increases the grains tend to grow following a 3D model. Therefore, the grain shape changes to a pyramidal structure. In short, the grain size increases and the grain shape changes from hexagonal to pyramidal as the film gets thicker. To calculate the optical band gap energies of the films, we used the absorption coefficient $\alpha \propto \ln(T/T_0)$ corresponding to the band gap of ZnO wurtzite structure. In Fig. 2, we plot $[\alpha(h\nu)]^2$ against the photon energy, $h\nu$. By extrapolating the linear region of these curves (at higher energies) we determined the optical gap value of the films as their intersections with the horizontal axis. The inset of Fig. 2 shows the obtained gap values as a function of film thickness. Interestingly, the band gap energy of the AZO layers decreased slightly with thickness. In general, band gap energy variations in ZnO thin films are related to changes in mean crystallite size, internal stress and/or free carrier concentration [Lin and Huang (2004); Banerjee et al. (2006); He et al. (2006); Suchea et al. (2007); Bouderbala et al. (2009)]. It is well-known that two competing phenomena affect the band gap energy values as donor density increases, mainly in heavily doped semiconductors [Lucio-López et al. (2006)]. The first is related to a gap widening due to the band-filling effect, known as Burstein-Moss effect [Roth et al. (1982)]. This phenomenon involves a gap widening in highly n-doped materials as the carrier concentration increases, owing to a blocking of lowest states of conduction band by excess electrons [Suchea et al. (2007)]. The second phenomenon affects the gap of ZnO for carrier concentrations above the Mott critical concentration ($\sim 5 \times 10^{18}$ cm^{-3}) because electron-electron and electron-impurity interactions give rise to an energy shift of the valence and conduction bands, reducing the band

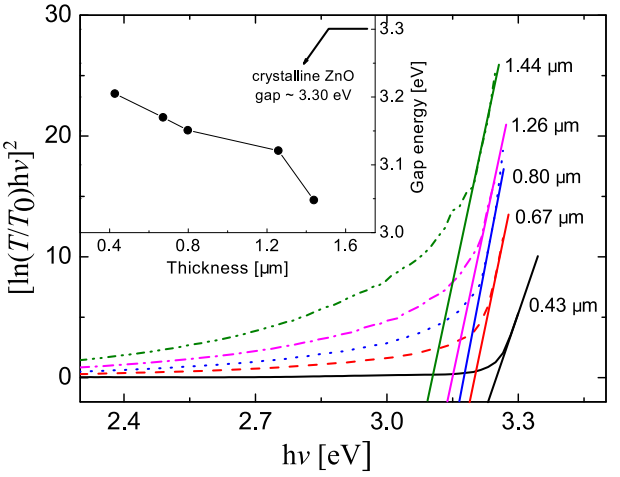

Fig. 2. Absorption coefficient curves of AZO films with different thicknesses. The inset presents the determined optical gap values.

gap [Lucio-López et al. (2006)]. This has been attributed to the merging of an impurity band into the conduction band, thereby shrinking the band gap. In many materials, this transition is observable as a disappearance of the conductivity activation energy. This feature was not observed for our samples, since the films are polycrystalline and the carrier mobility is dominated by grain boundary effects.

Our results indicate that the shrinkage effect is the dominant phenomenon, which is evidenced by the diminution of optical gap values (inset of Fig. 2) as thickness (and carrier concentration, as explained below) increases.

The XRD patterns of AZO films with different thicknesses are shown in Fig. 3. All samples presented the characteristic diffraction peaks of hexagonal wurtzite ZnO (JCPDS N° 36-1451). We have marked with an asterisk (*) the peak centered at $2\theta = 38.55°$, present in all patterns, which is due to a secondary $ZnAl_2O_4$ phase [Wei et al. (2013)]. The presence of strong and sharp peaks indicated that the films possessed crystalline domains. The thinnest sample presented three clear diffraction peaks, (1 0 1), (0 0 2) and (1 0 3), evidencing a strong orientation in the [0 0 2] direction. The preferential orientation of *c* axis in ZnO layers leads to an enhancement of the (0 0 2) diffraction peak [Lucio-López et al. (2006); Huang et al. (2001)]. When our films grew thicker than 0.80 μm, the (1 0 2) and (1 0 3) peaks appeared more defined, and the peak (0 0 2) remained as dominant. In turn, when the thickness increased

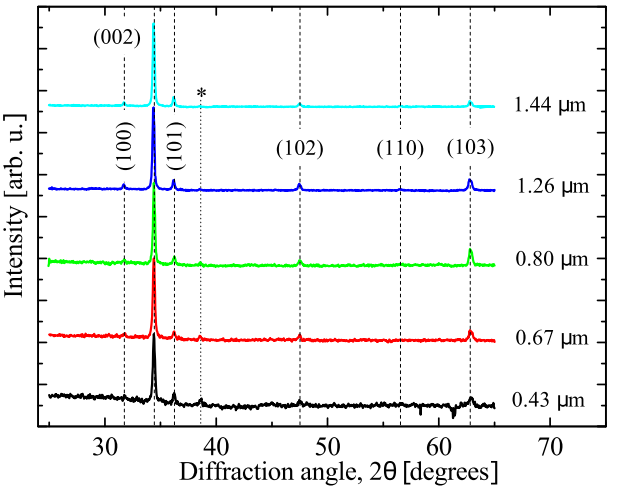

Fig. 3. X-ray diffraction patterns of AZO layers with different thicknesses, showing the characteristic ZnO crystalline peaks.

to around 1.44 μm (~ 30 min), the (0 0 2) diffraction peak was still dominant while the other peaks resulted slightly diminished. Some authors suggest that for thick enough AZO films, the surface tends to be oriented in the [0 0 2] direction due to its lower surface energy [Fujimura et al. (1993)].

The fact that such small intensities were observed for (1 0 1), (1 0 2) and (1 0 3) diffraction peaks, can be attributed to a growth competition between neighboring crystals according to their orientations. The faster growing crystals will grow over the slower ones. This competitive growth represents an orientation selection among the crystals and results in what is called the competitive growth texture [Lin and Huang (2004)], which explains the diminished intensity of these diffraction peaks in our samples [Kumar et al. (2005)].

To further investigate the difference between the films exhibiting a *c* axis or (0 0 2) preferential orientation and the intensity reduction of the other diffraction peaks, we performed mosaicity measurements by XRD. This allowed us to analyze the crystalline homogeneity of the material. The rocking curves around the diffraction angle of maximum intensity were obtained as described in a previous work [Garcés et al. (2013)].

Fig. 4 illustrates the full-width at half-maximum (FWHM) evolution of the rocking curves for the (0 0 2) peak as the thickness of AZO films increased. A typical rocking curve is showed in the inset of Fig. 4, for the 0.43 μm sample. The FWHM increased from 12.8° for a thickness of 0.43 μm to 18° for 0.80 μm. For the highest thickness (1.44 μm) the FWHM decreased to 15°. These FWHM values of the (0 0 2) rocking curves revealed the average uniformity of the *c* axis orientation throughout the volume of the films. A smaller FWHM means better uniformity in the orientation of the *c* axis and, consequently, better crystalline quality. The dependence of FWHM with thickness is also due to stress in the films.

When AZO films are grown by techniques like RF sputtering [Owen et al. (2012)] or laser ablation [Perrière et al. (2002); Dong et al. (2007)], using mono-crystalline substrates, the FWHM values extracted from the rocking curves have a different behavior in comparison to our films. This can be explained by the epitaxial growth mechanism during film deposition by these techniques. Thus, at the initial stages of deposition there is an important structural mismatch between the ZnO film and the substrate. This results in large strain within the epitaxially grown films, disturbing the uniformity of the *c* axis orientation. As the films grow, the strain between new layers and older ones is relaxed. Therefore, thicker films usually exhibit smaller FWHM values in their rocking curves and improved crystalline quality [Perrière et al. (2002)].

At a first place, the different behavior of FWHM values as a function of thickness in our films is attributed to the fact that AZO films do not grow epitaxially on the glass substrates. During initial growth stages, as said before, various grain orientations compete [Drift (1967)]. Also, the average grain size increases as the fastest growing grains dominate over differently oriented neighboring grains. In this case, the nucleation density is greater than the grain

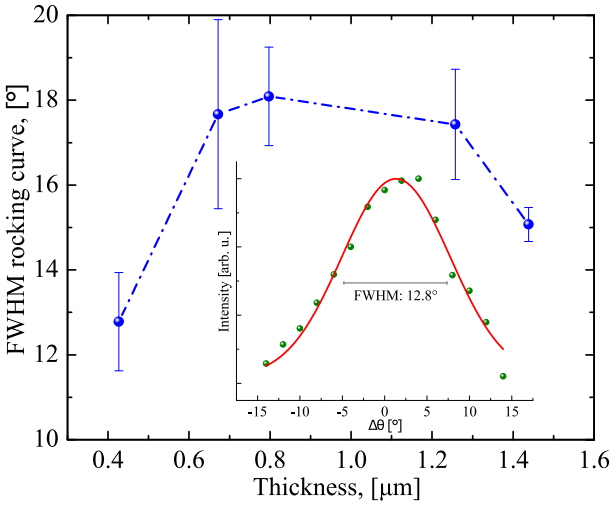

Fig. 4. Full-width at half maximum values of the rocking curves as a function of film thickness, determined for the (0 0 2) diffraction peak. The inset shows the fitting procedure (for the 5 min sample) to determine the FWHM value.

density. In our case, consequently, a maximum value of the FWHM was observed for the 0.80 μm-thick sample. This is attributed to the presence of grain boundaries, which increase the strain in the films. For thicker samples the strain is relaxed, as mentioned above, leading to a subsequent FWHM diminution. Therefore, the FWHM curve of Fig. 4 clearly shows a transition point from high to low strain in the films for a thickness of 0.80 μm.

As reported by Owen et al. (2012), the chemical termination of the surface affects the characteristics of the next layer during the growth process. The authors proposed a flipping of grain polarity from O-to Zn-termination during growth. This would cause that faster progressing Zn-terminated growth overtakes neighboring O-terminated material, leading to textured growth. In our samples, the different sizes of features on the surface (Fig. 1) would be due to the c axis polarity flipping at different points during growth.

In-plane stress of the films was calculated using the biaxial strain model [Maniv et al. (1982)]. This model involves a series or parameters, namely, interplanar spacing, d, corresponding in our case to (0 0 2) reflex in the XRD pattern, the corresponding spacing for a stress-free system, $d_0 = 0.2603$ nm, and elastic stiffness constants, C_{ij}. In this model, the stress is calculated as

$$\sigma = \left[2C_{13} - C_{33}\frac{C_{11}+C_{13}}{C_{13}}\right]\frac{d-d_0}{d_0}. \quad (1)$$

The values of d were calculated using the Bragg formula $2d\sin\theta = \lambda$, where θ is the Bragg angle corresponding to the (0 0 2) peak in the XRD pattern and λ is the wavelength of X-rays. The spacing d was found to vary with film thickness. After inserting the values of C_{ij} [Maniv et al. (1982)] in Eq. (1), the internal stress was calculated for each film and the resulting values are plotted in Fig. 5.

The negative sign of σ indicates that the stress in the films is compressive in nature. It may be noted that thermal stress arising due to differences in thermal expansion coefficients between the film (α-ZnO = 2.9×10^{-6} 1/K) and the substrate (α-glass = 7.2×10^{-6} 1/K), because the deposition process was made at 450 °C. Moreover, in general the internal stress varies during film growth as explained in the following paragraph.

Generally, in polycrystalline thin films, there are different regimes of internal stress during film growth. First, during the early nucleation stage (i.e. before the film has coalesced) compressive stress is attributed to the effect of surface capillary forces on isolated clusters [Cammarata et al. (2000)]. Subsequently, when these clusters coalesce, a tensile stress develops which is associated with the formation of grain boundaries [Sheldon et al. (2001)]. After further growth, to form a fully continuous film, this tensile stress decreases. The average stress continues decreasing until reversing its trend, i.e. changing from tensile to compressive (due to relaxation of the tensile component) [Sheldon et al. (2001)]. This is attributed to an increase in the surface chemical potential which is known to induce atoms to flow into grain boundaries, creating a compressive stress in the film [Chason et al. (2002)]. In this context, as is observed in Fig. 5, all films deposited in our work have compressive stress. We attributed this to the fact that the transition between tensile to compressive stress takes place for a film thickness of 10 nm. For thicker films, compression persists due to atoms flowing to grain boundaries [Cammarata et al. (2000); Sheldon et al. (2001); Chason et al. (2002)].

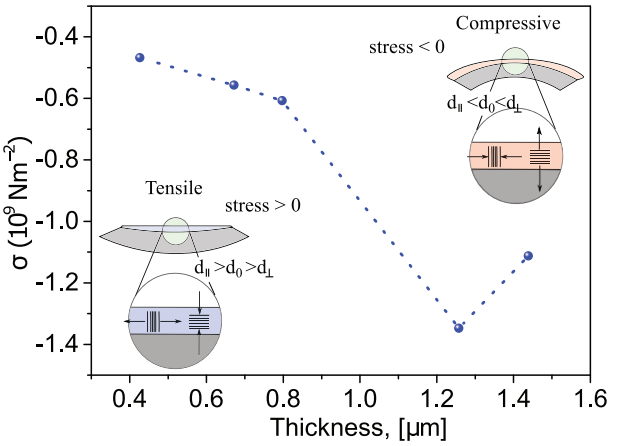

Fig. 5. Plot of in-plane stress (σ) of films as a function of thickness.

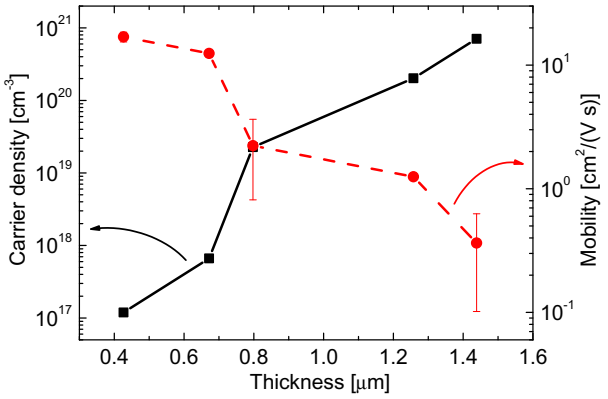

Fig. 6. Carrier concentration (n) and Hall Mobility (μ) as a function of thickness. Lines are only a guide to the eye.

Fig. 6 shows the variation of carrier concentration and Hall mobility as a function of thickness. We could see an exponential increase of carrier concentration as samples thickened, of about three orders of magnitude. On the other hand, there was a decrease of carrier mobility. Therefore, the carrier concentration shown in Fig. 6 accounts for all free electrons excited from Al atoms and native defects. In consequence, we conclude that Al atoms and native defects, both acting as donors, increased free carrier concentration as the films thickened.

On the other hand, the ZnO films showed high resistivity due to chemisorption of oxygen [Igasaki and Saito (1991); Rao and Santhoshkumar (2009)] at grain boundaries (we recall that air was used as gas carrier during deposition). When the deposition is performed at low temperatures ($\sim$ 150 °C), oxygen is chemisorbed in the film both at grain boundaries and at the surface [Igasaki and Saito (1991)]. The rapid cooling at the end of deposition does not allow oxygen to escape from the sample. However, considering the higher temperature used in this work (450 °C), oxygen would have more available thermal energy to escape and increase the final carrier concentration of the samples. So, adsorbed oxygen may produce potential barriers which hinder the electrical transport. The principal chemisorption species in ZnO are O_2^{-1} at low temperatures. When deposition temperature raises, the chemisorbed O_2^{-1} desorbs from the sample and donates an electron to ZnO (i.e. $O_2^{-1} \longrightarrow O_2 + e^-$) [Rao and Santhoshkumar (2009)]. This reaction produces a diminution of film resistivity. Besides this, we can consider that the surface area of the sample increases as it thickens, which also increases the fraction of free electrons trapped by chemisorbed oxygen and subsequently donated during oxygen desorption. This fact was evidenced by the results showed in Fig. 2, where the shift in the absorption edge was attributed to a higher carrier concentration [Roth et al. (1982); Sernelius et al. (1988)]. As is also observed in Fig. 6, Hall mobility decreased for thicker samples. Carrier mobility is related to macroscopic and microscopic imperfections in the films. At the macroscopic level we include grain boundaries, internal stress and surface roughness, all of which can be observed in XRD and AFM measurements. In turn, the microscopic level accounts for ionized donors and neutral impurity atoms. In ZnO, particularly, a surface barrier is created by the chemisorption of oxygen, which considerably reduces carrier mobility. Besides this, grain boundaries are also considered to be effective inhibitors of carrier mobility [Igasaki and Saito (1991)].

Carrier mobility in thinner AZO films, with lower RMS roughness, resulted strongly dependent on thickness. However, it remained constant for thicknesses between 0.80 and 1.26 μm. We consider that the thickness dependence of mobility in AZO films is mainly due to a variation in the density of scattering centers, such as lattice strain points, and dislocations caused by misorientations between crystalline domains (mosaicity). The mobility of the thickest film (1.44 μm) reached a minimum value, although the FWHM value of its rocking curve was slightly lower than for the 1.26 μm sample. This might be indicating that the defect density increased for higher deposition times and that other scattering centers (such as grain boundaries) were introduced in the film. Thus, we conclude that the density of scattering centers increases with deposition time, resulting in reduced carrier mobility.

In view of the results presented above, it is believed that in-plane stress in the film is mainly responsible for a shift in the gap energy. As the thickness of the film decreased (layer with 0.43 μm), the stress was relaxed and gap energy approached a value expected for stress-free state (intrinsic value). For films with high carrier concentration (thickest layer) there was an increase in surface chemical potential inducing atoms to flow into the grain boundary (high

compressive stress and high misorientation between crystalline domains), generating defect points and promoting the oxygen chemisorption at grain boundaries.

4. Conclusion

We have obtained Al-doped ZnO thin films on glass with different thicknesses through sol-gel synthesis and spray pyrolysis deposition at 450 °C. We have analyzed the correlation between morphological characteristics, like RMS roughness, grain size, preferential growth orientation, residual stress and mosaicity, with electrical characteristics, like mobility and carrier concentration, and their evolution with film thickness. In all samples, we obtained low resistivities, in the order of 10^{-1} Ω cm, and moderate Hall mobilities, of about 5 $cm^2/(V\ s)$. We found that by increasing film thickness the mosaicity between crystalline domains results greater and the compressive stress is high. This has a direct influence on resistivity and carrier concentration, since thicker films yielded lower resistivities and higher carrier concentrations. Also, the optical gap energy showed a blue shift. Therefore, the results presented demonstrate the strong influence the spray pyrolysis growth parameters have on the electrical properties of the ZnO thin films. In particular, the thickening effect has a marked effect on carrier concentration.

Acknowledgements

This work was partially supported by projects from ANPCyT (PICT 32515), Universidad Nacional del Litoral (CAID 2009/68-343) and CONICET (PID 1464). We also acknowledge Ramón Saavedra.

References

Bagnall, D.M., Chen, Y.F., Zhu, Z., Yao, T., Koyama, S., Shen, M.Y., Goto, T., 1997. Appl. Phys. Lett. 70, 2230.
Banerjee, A.N., Ghosh, C.K., Chattopadhyay, K.K., Minoura, H., Sarkar, A.K., Akiba, A., Kamiya, A., Endo, T., 2006. Thin Solid Films 496, 112.
Biswal, R.R., Velumani, S., Babu, B.J., Maldonado, A., Tirado-Guerra, S., neda, L.C., de la L. Olvera, M., 2010. Mat. Sci. Eng. B 174, 46.
Bouderbala, M., Hamzaoui, S., Adnane, M., Sahraoui, T., Zerdali, M., 2009. Thin Solid Films 517, 1572.
Cammarata, R.C., Trimble, T.M., Srolovitz, D.J., 2000. J. Mater. Res. 15, 2468.
Chason, E., Sheldon, B.W., Freund, L.B., 2002. Phys. Rev. Lett. 88, 156103–1.
Choi, J.H., Tabata, H., Kawai, T., 2001. J. Cryst. Growth 226, 493.
Dong, B.Z., Fang, G.J., Wang, J.F., Guan, W.J., Zhao, X.Z., 2007. J. Appl. Phys. 101, 033713.
Drift, A.V.D., 1967. Philips Res. Rep. 22, 267.
Ellmer, K., 2000. J. Phys. D: Appl. Phys. 33, R17.
Fujimura, N., Nishihara, T., Goto, S., Xu, J., Ito, T., 1993. J. Crystal Growth 130, 269.
Garcés, F.A., Budini, N., Koropecki, R.R., Arce, R.D., 2013. Thin Solid Films 531, 172.
Gorla, C.R., Emanetoglu, N.W., Liang, S., Mayo, W.E., Lu, Y., Wraback, M., Shen, H., 1999. J. Appl. Phys. 85, 2595.
Granqvist, C.G., 2007. Sol. Ener. Mat. Sol. Cells 91, 1529.
Hao, X.T., Zhu, F.R., Ong, K.S., Tan, L.W., 2006. Semicond. Sci. Tech. 21, 48.
He, H.P., Zhuge, F., Ye, Z.Z., Zhu, L.P., Wang, F.Z., Zhao, B.H., Huang, J.Y., 2006. J. Appl. Phys. 99, 023503.
Huang, M.H., Mao, S., Feick, H., Yan, H., Wu, Y., Kind, H., Weber, E., Russo, R., Yang, P., 2001. Science 292, 1897.
Igasaki, Y., Saito, H., 1991. J. Appl. Phys. 70, 3613.
Kumar, P.M.R., Kartha, C.S., Vijayakumar, K.P., Abe, T., Kashiwaba, Y., Singh, F., Avasthi, D.K., 2005. Semicond. Sci. Technol. 20, 120.
Lan, S.M., Uen, W.Y., Chan, C.E., Chang, K.J., Hung, S.C., Li, Z.Y., Yang, T.N., Chiang, C.C., Huang, P.J., Yang, M.D., Chi, G.C., Chang, C.Y., 2009. J. Mater. Sci.: Mater. Electron. 20, 441.
Lin, S.S., Huang, J.L., 2004. Surf. Coat. Technol. 185, 222.
Lokhande, B.J., Uplane, M.D., 2000. Appl. Surf. Sci. 167, 243.
Lucio-López, M.A., Maldonado, A., Castanedo-Pérez, R., Torres-Delgado, G., de la L. Olvera, M., 2006. Sol. Ener. Mat. Sol. Cells 90, 2362.
Maniv, S., Westwood, W.D., Colombini, E., 1982. J. Vac. Sci. Technol. 20, 162.
Mekhnache, M., Drici, A., Hamideche, L.S., Benzarouk, H., Amara, A., Cattin, L., Bernède, J.C., Guerioune, M., 2011. Superlattices and Microstructures 49, 510.
Minami, T., 2008. Thin Solid Films 516, 5822.
Natsume, Y., Sakata, H., 2000. Thin Solid Films 372, 30.
Owen, J.I., Zhang, W., Köhl, D., Hüpkes, J., 2012. J. Crystal Growth 344, 12.
Paraguay D., F., Morales, J., Estrada L., W., Andrade, E., Miki-Yoshida, M., 2000. Thin Solid Films 366, 16.
Perrière, J., Millon, E., Seiler, W., Boulmer-Leborgne, C., Craciun, V., Albert, O., Loulergue, J.C., Etchepare, J., 2002. J. Appl. Phys. 91, 690.
Rao, T.P., Kumar, M.C.S., Hussain, N.S., 2012. J. Alloys and Compounds 541, 495.

Rao, T.P., Santhoshkumar, M.C., 2009. Appl. Surf. Sci. 255, 4579.
Roth, A.P., Webb, J.B., Williams, D.F., 1982. Phys. Rev. B 25, 7836.
Sernelius, B.E., Berggren, K.F., Jin, Z.C., Hamberg, I., Granqvist, C.G., 1988. Phys. Rev. B 37, 10244.
Sheldon, B.W., Lau, A., Rajamani, A., 2001. J. Appl. Phys. 90, 5097.
Suchea, M., Christoulakis, S., Katsarakis, N., Kitsopoulos, T., Kiriakidis, G., 2007. Thin Solid Films 515, 6562.
Wei, T., Zhang, Y., Yang, Y., Tan, R., Cui, P., Song, W., 2013. Surf. Coat. Technol. 221, 201.
Znaidi, L., 2010. Mat. Sci. Eng. B 174, 18.